ORIGINAL PAPER

Exploring Factors Influencing the Inhibitory Effect of Volume Dielectric Barrier Discharge on Phytopathogenic Fungi

Palma Rosa Rotondo[1] · Domenico Aceto[2] · Caterina Rotolo[1] ·
Marianna Ambrico[2] · Giorgio Dilecce[2] · Francesco Faretra[1] ·
Rita Milvia De Miccolis Angelini[1] · Paolo Francesco Ambrico[2]

Abstract

The application of Low-Temperature Plasmas has shown great potential as an effective and alternative tool for microbial inactivation in recent years. Nevertheless, further investigations are required to fully understand the possible factors influencing these processes. The present study aims to investigate the effectiveness of square wave modulated Volume Dielectric Barrier Discharge on the direct inhibition of conidial germination in five different fungal species, various discharge conditions, and medium composition. The five different fungal species used were *Botrytis cinerea, Monilinia fructicola, Aspergillus carbonarius, Fusarium graminearum*, and *Alternaria alternata*. On water agar, the inhibition of *Botrytis cinerea* was influenced by the applied voltage, which mainly reflects the uniformity of the treatment. Under the selected voltage condition, the inhibition increased with treatment duration and decreased with fungal spore complexity. *B. cinerea* and *M. fructicola*, with unicellular conidia and low melanin content, showed similar behaviour and high sensitivity to the treatment. *F. graminearum* and *A. alternata*, both having multicellular conidia, were more resistant to the plasma treatment and showed different sensitivity likely due to different content in melanin. However, after 1 min of treatment, complete inhibition of conidial germination was achieved for all the tested species. Inhibition of *A. carbonarius* conidia on different agarized media containing dextrose or malt extract was influenced by the complexity and composition of the medium, being potato dextrose agar that more hindered the plasma efficacy. Each medium exhibited a different electrical response studied by Electrical Impedance Spectroscopy and morphology observed by Scanning Electron Microscopy images. These differences translated into a different response to the applied electrical field, influencing plasma generation and uniformity.

Keywords Low-temperature plasma · VDBD · Microorganism · Decontamination · SEM

Extended author information available on the last page of the article

Introduction

Plasma is a partially ionized gas containing atoms or molecules in a metastable state with a roughly zero net electrical charge [1]. Non-equilibrium plasmas generated at room temperature, under either low or atmospheric pressure in ambient or synthetic air, nitrogen, oxygen, helium, hydrogen, argon or their mixtures can operate at a near room temperature obtaining the so-called Low-Temperature Plasma (LTP) or Cold Plasma [1]. The plasma state is reached by applying a strong electric field to the gas mixture, and many plasma sources are currently available. Among non-equilibrium atmospheric pressure plasmas, Dielectric Barrier Discharges (DBDs) are the most promising ones for applications on biological tissues. DBDs consist of metallic electrodes, one or both covered by dielectric plates separated by a distance (usually from 10^{-3} to 10^{-2} m) with the working gas occupying this inter-dielectric space. When a high voltage is applied to the electrodes, generally from 10^2 to 10^4 V depending on gas and pressure, with frequency from 10^0 to 10^4 Hz, the gas in the gap experiences an increase in voltage and gas ionization is on-set [2].

In recent years, LTP application has shown great potential as an effective and alternative tool for microbial inactivation on food and agricultural products, based on sustainability, human safety, and long-term eco-safety [3–5]. The activated chemical species of LTP can act rapidly against pathogenic and food-spoiling microorganisms at room temperature without leaving any known chemical residues [6]. Plasma generates charged particles and various levels of reactive oxygen and nitrogen species (RONS) that act on multiple target sites causing loss of function, structural damage and ultimately cell death [7, 8]. The antimicrobial effect of different LTPs, however, depends on several factors such as feed gas composition, relative humidity, power supplied, and treatment time [9]. In particular, treatment time and power used for plasma generation are important parameters that could affect the efficacy of the treatment [4]. Bacterial and fungal target species show different levels of sensitivity to plasma treatments, depending on their biological traits. Differences in cell and sub-cellular structures, and metabolism are involved in the response of each microorganism to plasma treatment [7]. Many fungi produce different pigments and especially melanin that may protect from damaging agents such as UV irradiation, desiccation, extreme temperatures, and strong oxidants [10–12]. Therefore, conidia with different melanin content in the cell wall layers could show different sensitivity to plasma treatment.

This study was aimed at evaluating the influence of several parameters on the effectiveness of a Volume Dielectric Barrier Discharge (VDBD) in inhibiting conidial germination in five selected phytopathogenic fungi: *Alternaria alternata*, causing black spots in many fruits and vegetables; *Aspergillus carbonarius*, responsible for bunch rot and ochratoxin A contamination of grapes and derived products; *Botrytis cinerea*, causing the grey mould disease on numerous crops; *Fusarium graminearum*, a major pathogen of cereal crops and producing several mycotoxins; and *Monilinia fructicola*, inducing brown rot on stone fruit. These five fungal species are ubiquitous plant pathogens, causing heavy yield losses either in the field or in post-harvest, straightening food quality and safety, and often difficult to control.

In this work, we critically studied the parameters possibly affecting the efficacy of plasma treatment on each of the selected fungal species. The differences in treatment time required for the complete inhibition were related to plasma behaviour in different agarized media, plasma emission and temperature, the electrical response of the plasma and different

biological traits of the analyzed fungi. Moreover, we focussed also on the possible effect of medium composition and structural properties using Electrical Impedance Spectroscopy (EIS) and Scanning Electron Microscopy.

Materials and methods

Discharge System

The current setup was realized to evaluate the in vitro efficacy of volume plasma treatments on conidial germination. The reactor is designed for lab scale processes on biological samples (a similar one was used on seeds [13]), upscale in the size should be considered for practical applications. The volume barrier discharge was realized by a 3D-printed reactor whose main concept is reported in Fig. 1. The reactor is equipped with gas in and gas out feedthrough, UV optical windows.

The configuration adopted was made of a double barrier DBD: nickel paint was used to realize metallic electrodes ($\varphi = 6$ mm) by screen printing technique on the opposite surface of the two circular alumina plates ($\varphi = 25.4$ mm) that act as a dielectric barrier. The alumina disks were mounted on sliding supports that allow the insertion and removal of the samples from the chamber. The samples were positioned in a sample holder on the grounded electrode, while fixed spacers were used to keep the discharge electrode distance constant at about 6 mm. The optical axis was defined by the discharge gap centre and the centre of UV-grade fused silica windows. The optical axis, discharge axis and gas flow direction were mutually orthogonal. The VDBD was powered by an AC power supply composed of a TTI TG1010A 10 MHz DDS Function Generator to generate the low voltage AC cycles, TTI TG5011A 50 MHz Pulse generator to trigger the low voltage waveform, a Powertron Model 1000 A RF Amplifier and a high-voltage step-up transformer to generate the HV waveform.

The discharge was working in burst mode to prevent overheating of the treated samples and keep the gas temperature on average as close as possible to room one. Bursts composed of two cycles of a 5 kHz sine-wave AC HV waveform (Fig. 1(B)) were sup-
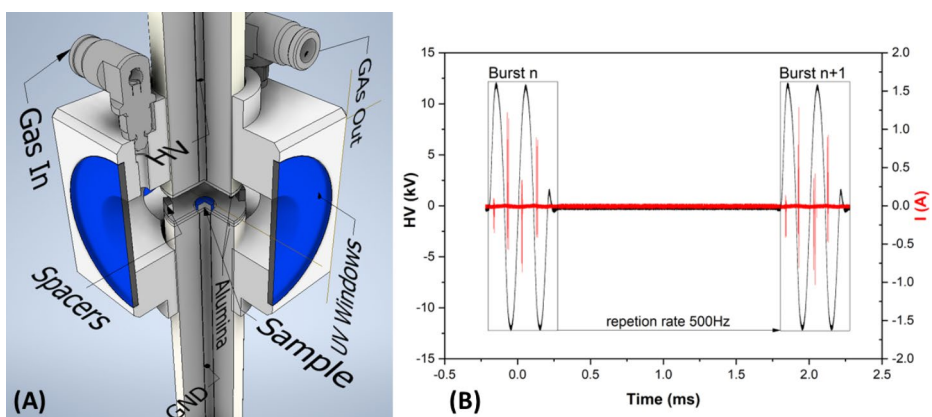

Fig. 1 (A) Volume dielectric barrier discharge schematic, (B) Applied voltage waveforms and measured current

plied to the discharge with a repetition rate of 500 Hz, with a nominal fixed duty cycle $D = T_{ON}/(T_{ON}+T_{OFF}) = 20\%$. The treatment time was precisely selected by programming the TTi TG5011A Pulse Generator in burst mode with a repetition rate of 500 Hz and a $number\,of\,burst = 500\,Hz \times treatment\,time\,(s)$.

A Keysight InfiniiVision MSOX6004A (bandwidth 1 GHz, up to 20 GS/s) was used to record the discharge voltage–charge and voltage-current characteristics. A Tektronix P6015A high voltage probe (1,000:1@1 MΩ, Bandwidth 25 MHz, rise time 4.7ns) was used to measure the applied voltage, a Magnelab CT-c1.0 Rogowski coil (rise time 0.7 ns) on the ground cable was used to measure the current, and a 2.4 nF high voltage capacitor inserted between the induction electrode and the ground was used to derive charge measurements, respectively. The energy was measured from charge-voltage Lissajous characteristics by integrating them. The reactor was fed with ambient humid air (RH 40%, $T_{amb} = 24\,°C$) at a fixed flow rate of 7 slm.

Emission Spectroscopy

UV-grade quartz frontal windows allow direct visual control of the discharge area and optical emission diagnostics. Optical emission spectroscopy was performed by collecting light from the plasma with an optical system composed of two 30 cm focal length UV grade quartz lenses that focus the plasma emission from the discharge gap on the entrance slit of the monochromator. The collected light is limited by the entrance slit width of the monochromator and can reach a maximum dimension of 3 (width) × 5 (height) mm^2. The light is spectrally resolved by a 30 cm spectrometer (Acton Spectra Pro 2300), equipped with a multiple-grating turret (300/600/1200 grooves×mm^{-1}, blazed at 300 nm) and a Princeton Instruments PI-MAX4 1024i CCD (1024×1024 pixel sensor, pixel size 12.8 µm, active area 13.1×13.1 mm^2). One CCD image of a spectrum covers a range of approximately 144/65/30 nm respectively for the three different gratings. The intensities of the emission spectra, acquired by the ICCD (Intensified CCD) detector, were spectrally and intensity corrected through calibration and Halogen lamps, and collected at the beginning of each HV half cycle with a 50 µs gate starting (see details in the results section).

Fungal Strains, Growth Conditions And Plasma Treatment

The antifungal efficacy of VDBD plasma treatment against strains of five fungal species was evaluated by standard in vitro conidial germination tests. *B. cinerea* strain SAS56, *M. fructicola* strain Mfrc123, *A. alternata* strain Alt1, *F. graminearum* strain 272 F and *A. carbonarius* strain AC49 were maintained in our fungal collection. The cultures, stored in aqueous 10% glycerol at -80 °C, were revitalized on potato dextrose agar [PDA: infusion from 200 g peeled and sliced potatoes kept at 60 °C for 1 h, 20 g D(+)-glucose, adjusted at pH 6.5, 20 g agar Oxoid No. 3; per litre]. For conidia production, colonies were grown on PDA at 21±1 °C, exposed to a combination of two daylight (Osram, L36W/640) and two near-UV (Osram, L36/73) lamps. Conidia suspensions were obtained by scraping the surface of seven-day-old colonies in sterile distilled water, filtered through glass wool to remove mycelial fragments and adjusted to 0.5-1×10^5 conidia mL^{-1} by using a hemocytometer. Aliquots (10 µL) of conidial suspension were then spotted on Water Agar (WA: 20 g L^{-1} agar Oxoid No. 3) disks of 6 mm of diameter, placed on sterile microscope slides

and submitted to the plasma treatment in the sample holder of the reactor described before. For *A. carbonarius*, showing a very low germination rate (< 20%) on WA, different agarized media were used: Agar Glucose (AG: 10 g L^{-1} D(+)-glucose, 20 g L^{-1} agar Oxoid No. 3); Malt Extract Agar (MEA: 20 g L^{-1} malt extract, 20 g L^{-1} agar Oxoid No. 3); and PDA.

For all the five fungal species tested, the overall exposure times used were 0.5, 1, 2, 5, 10, 20, 30, 60 and 180 s corresponding to a nominal plasma on time of 0.1, 0.2, 1, 2, 4, 6, 12, 36 s, respectively. The response to plasma energy was also explored by changing the HV and using *B. cinerea* as reference fungal species and an exposure time of 30 s. Treated and untreated media disks inoculated with untreated conidia were used as negative controls. The disks were then incubated in a moist chamber at 25 ± 1 °C in the dark. After 18 h, microscopic observations were conducted at ×200 magnification on random samples of 100 conidia from three replicated spots for each condition. The inhibition rate (%) caused by plasma treatment was calculated on the ground of the percentage of germinated conidia on the unexposed control disks.

Cryo-SEM Imaging

SEM images of disks of different agarized media were acquired employing a Hitachi TM 3000 series desktop Cryo-SEM apparatus. The technique is based on freezing the samples down to -40 °C on the SEM Peltier Cryo-stage (Coolstage) and setting it for observation in the SEM vacuum chamber. Once in the vacuum, a proper temperature increases at about $-28/-22$ °C allows external ice sublimation and exposes the frozen sample to direct SEM imaging. The technique does not need critical point drying or metal coating and retains the natural structure of samples allowing observation of surface and section morphology.

Impedance Spectroscopy Characterization And data Analysis

Impedance (Z) vs. frequency (f) spectra were collected on slabs of WA, AG, MEA and PDA (0.8×0.8×0.4 cm) using a plane parallel capacitor configuration by placing each sample of agarized media between two conductive electrodes (Au foil and ITO/glass, 0.8×0.8×0.4 cm). The Electric Impedance Spectroscopy (EIS) spectra were recorded by a NOVOCONTROL impedance analyser in the frequency range $10^{-1} - 10^{7}$ Hz by applying an AC voltage of 300 mV and a DC bias V_{DC}= 2.5 V producing an ionic charge current across the media. The measurements were performed under ambient air conditions, at a relative humidity of 40% at 24 °C.

The EIS measurements returned the modulus (|Z|) and phase angle (φ) of the impedance (Z) as a function of the frequency (f) of the AC signal. The recorded impedance was plotted as a Nyquist plot (NPs), i.e., where ReZ, and -ImZ, are respectively the real and imaginary parts of Z. In this representation, the frequency increases going from the right to the left of the NPs [14]. The data have been subsequently fitted to the impedance of a proper electrical circuit by adopting a free downloadable EIS analyser software [15, 16].

Statistical Analysis

Data were analysed by ANOVA and Tukey's HSD (Honestly Significant Difference) test to compare all pairs of means at 0.05 and 0.01 probability levels (*P*) using CoStat software (CoHort Software, Monterey, CA).

Results

Optical Emission Spectroscopy

Plasma Induced Emission (PIE), collected orthogonally with respect to the gas flow, showed the characteristics of streamer-based discharges. PIE was observed from the middle of the discharge gap and collected with an ICCD gate of 50 µs starting at the beginning of each HV half cycle (see Fig. 2A).

PIE evidenced the asymmetric geometry of the discharge due to the presence of an agarized medium on the ground electrode. PIE spectra in the UV spectral range revealed strong bands of the molecular nitrogen second positive system (SPS) ($C^3\Pi_u \rightarrow B^3\Pi_g$), and of the N_2^+ ion first negative system (FNS) ($B^2\Sigma_u^+ \rightarrow X^2\Sigma_g^+$) (Fig. 2C). In the vis-NIR range, the bands of the N_2 first positive system (FPS) ($B^3\Pi_g \rightarrow A^3\Sigma_u^+$) together with atomic oxygen (O) emission were detected. The SPS and FNS bands contain interesting information on the physical parameters of the discharge. From the SPS(0,0) band the rotational temperature was derived by using the spectroscopic tool Massive OES [17–19]. Figure 2B shows the experimental SPS(0,0) band profile together with synthetic profiles simulated for rotational temperatures of 340 K, 440 K, 480 K, and 640 K respectively for the PIE observed in the corresponding gates. The estimated error from multiple simulation of bands, not shown for the sake of clarity, at different temperature was on average of the order of 10% of the reported measurements being respectively ±55, ±44, ±42, ±70. We must point out that, due to the filamentary character of the discharge, the temperature measured by optical emission is not representative of the entire volume of the gas inside the chamber but only of the portion of the gas crossed by the streamer. Thus, we can intend this temperature the gas temperature only if the entire region was filled by streamers at the same time.

From the ratio of the FNS and SPS bands the reduced electric field (E/N) could be measured, according to the methodology described in [20], with the proper molecular data. Finally, the vibrational temperature of the nitrogen ground state could be estimated from the whole vibrational manifold of the SPS bands using the model of ref. [21, 22]. A summary of the results is given in Table 1, for the four spectra shown in Fig. 2C.

We remind that in the positive polarity halfwaves of gates 1 and 3 the disk of agarized medium acted as the temporary cathode. From the current waveforms, it is soon clear that the discharge was much less efficient in this case, with a small number of micro-discharges (streamers). This condition corresponds to a relatively small E/N. On the contrary, when it acted as the temporary anode, i.e., in the negative polarity halfwaves of gates 2 and 4, a much larger number of streamers was observed, with much higher energy deposition, and a comparatively higher electric field.

The E/N and average energy values are consistent with what can be found in the literature. Here we mention that E/N and electron energy distribution function (EEDF), from which
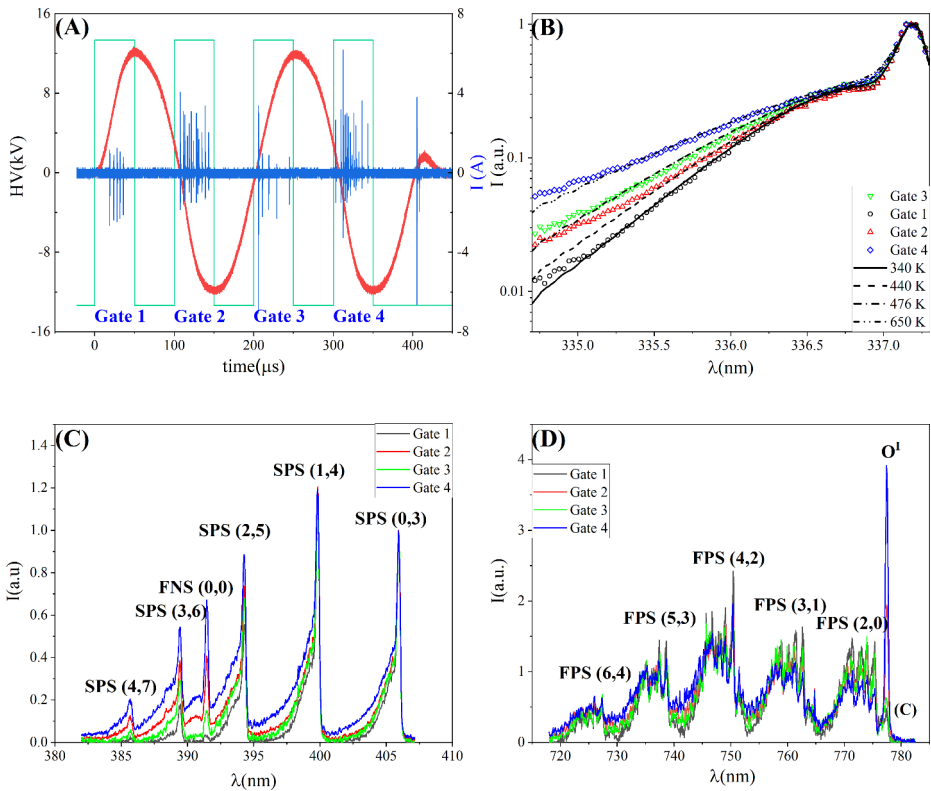
Fig. 2 (A) Voltage (red) and current (blue) characteristics of the discharge, and the gating scheme (light blue) labelled as Gate1, 2, 3, and 4, used to acquire the time-averaged molecular nitrogen spectra; (B) N_2 SPS(0,0) experimental band profiles complemented with synthetic profiles simulated for rotational temperatures T_{rot} of 340, 440, 480, 640 K. (C) SPS and N_2^+ FNS emission spectra of VDBD plasma; (D) FPS spectra and atomic oxygen emission line at 777 nm. All spectra averaged were taken with 1200 G/mm gratings (input slit width of 50 μm) over 1000 samples with a gate of 50 μs and corrected for the instrumental sensitivity

Table 1 Plasma parameters derived from emission spectroscopy at the four different gates as defined in Fig. 2(A). The E/N values are obtained by the analysis of the band ratios [20] using the quenching rate coefficients of [23]. In parenthesis, instead, we report the values obtained by using the quenching rate coefficients of [24] (see text)

Gate	HV Polarity	E/N (Td)	Electron average energy (eV)	T_{gas} (K)	T_{vib}(K)
1	Positive	220 (170)	5.7	340	2,400
3	Positive	390 (250)	8.3	480	3,400
2	Negative	560 (340)	11.36	440	4,000
4	Negative	680 (400)	12.3	640	5,200

the average energy are calculated, are tied to each other by the solution of the Boltzmann equation in the local field hypothesis. Here we use the Boltzmann solver BOLSIG+ [25]. In [26], the maximum electric field found in a positive streamer in air at 33 mbar was 500 Td. Note that here we observe a spatio-temporal average of the emission, and that most of the

emission comes from the space and time regions with higher electric field. In view of this, our E/N values are more representative of the higher E/N, although they must be somewhat lower than the maximum value. One must also consider that the measurements of [26] are at much lower pressure, where the streamer is bigger, which means lower local electric fields. An E/N measurement in the micro-discharge of a DBD discharge in dry air at atmospheric pressure was made in [27], where maximum values of E/N were in the range 400–450 Td. In that paper the calibration procedure outlined in [28] was used. The calculations in [28] used the collision quenching rate constants of [29], which are much lower than those we have used here, that are taken from [30]. Namely they are about 4 times and two times smaller for collision with nitrogen and oxygen, respectively. If we recalculate the E/N values with the collision data set of [29], we get the values in parenthesis reported in Table 1. We see that our measured bands ratio is consistent with that of [31], while the big discrepancy between the quenching rate constants determines the difference between the E/N values (and then average energy) calculated from the bands ratio. The reason why we prefer the rate constants of [30] can be found in the same paper and in [20]. It is not the case here to report the long discussion on the quenching rate constants used in the spectroscopic method for E/N measurement. The interested reader is directed to [20] and [32]. Here, after having given a flavour of the uncertainties in the E/N and average electron energy reported in Table 1, we discuss the trend of these parameters in the four measurement gates.

We propose the following scenario. The agarized medium is a less efficient emitter of secondary electrons than the bare-dielectric electrode. The secondary electrons initiate an avalanche that eventually evolves into a streamer. A small number of secondary electrons implies a small number of avalanches and smaller local charges at the avalanche head, which explains the lower E/N. In turn, such a lower E/N value determines a lower number of avalanches that evolve into a streamer. Very likely, these will be cathode-directed streamers. In the gates 2 and 4 halfwaves, instead, more avalanches and higher E/N initiate a massive evolution into streamers, perhaps even anode-directed since the Meek criterion can be satisfied even before the gap has been entirely crossed by the avalanches. The gas and vibrational temperatures increase accordingly, more in gates 2 and 4 than in 1 and 3 halfwaves, with a build-up from 1 to 3 and from 2 to 4. There is also a substantial increase in E/N between 1 and 3 and between 2 and 4. There can be two reasons: the first one is an increase of the initial electric field in the gap due to surface charge accumulation, which seems to be substantial between 1 and 3 since in halfwave 2 the current is much larger; the second reason is the decrease of the density (N) in the E/N ratio due to the gas temperature increase.

In the spectra of Fig. 2D, we observed the FPS bands and, in the gates 2 and 4 halfwaves, the oxygen atom 777 nm line. The FPS bands did not evidence anything of interest but the increase of the rotational temperature, in line with the SPS bands. The appearance of the O line was certainly linked to the higher current, the higher E/N and, therefore, the much higher dissociation of the oxygen molecules. The intensity of the atomic oxygen line, on the other hand, depends also on the electron energy, i.e. on E/N. The fact that the O line was not observed in the gates 1 and 3 halfwaves depends in part on the smaller electron-impact excitation rate. The same applies to the intensity difference between the lines in the gates 2 and 4 halfwaves: part of it could be due to an increase of the excitation rate with a higher E/N, not only to an increase of the O atoms density.

Influence of Applied Voltage on Antifungal Efficacy

Tests performed by applying an alternating electric field or DC electric field under similar AC plasma conditions with no plasma ignition did not produce a significant inhibitory effect on the conidial germination of all tested fungi (data not shown). Antifungal activity on *B. cinerea* conidia by plasma treatments was tested at different peak-to-peak voltages of the applied HV AC waveform keeping the treatment time fixed at 30 s. The results are reported in Table 2 and graphically shown in Fig. 3.

As expected, increased inhibition of conidial germination on WA was caused by increasing the AC peak-to-peak voltage of the electric discharges which translates into a raise of the energy per burst and consequently of the total energy supplied to the treated sample.

The effect of increasing energy doses on conidial germination seemed to follow a dose-dependent curve that reached a maximum plateau at 1.9 mJ per burst (23 kV$_{pp}$). Visual observations of the sample and the behaviour of the plasma during treatments were conducted. For voltage below 22 kV$_{pp}$, the plasma showed a marked localized behaviour with streamers mostly hitting some areas of the sample surface, leaving others almost untouched. This was also evidenced by microscopic observations of the treated samples that showed great variability of the effect of the treatment on conidia with complete inhibition of germination in some areas of the medium and germinated conidia in other areas, likely unexposed to plasma. At higher voltages, at least 23 kV$_{pp}$, the germination of conidia was completely inhibited on the entire disk surface.

Efficacy of Plasma Treatments on Different fungi

The treatments with VDBD plasma significantly inhibited the conidial germination of *B. cinerea*, *M. fructicola*, *F. graminearum* and *A. alternata* (Fig. 4). Pre-treatment of WA disks at the maximum treatment time (180 s) before conidia inoculation did not affect their germination (data not shown).

This demonstrates that possible modifications of the culture media chemistry due to plasma did not cause any inhibition of conidial germination.

Variance analysis (ANOVA) of data on the inhibition of conidial germination caused by VDBD showed that both the principal factors, fungal species and exposure time, as well as their interaction were statistically significant (Fig. 4; Table 3). The inhibitory effect

Table 2 Percentages of inhibition±standard error of germination of *B. cinerea* conidia exposed to different energy per burst (mJ) for a total number of 15,000 bursts corresponding to a total treatment time of 30 s. Figures followed by the same letter on the column, are not statistically different at the probability levels $P=0.05$ (small letters) or $P=0.01$ (capital letters) according to Tukey's HSD test

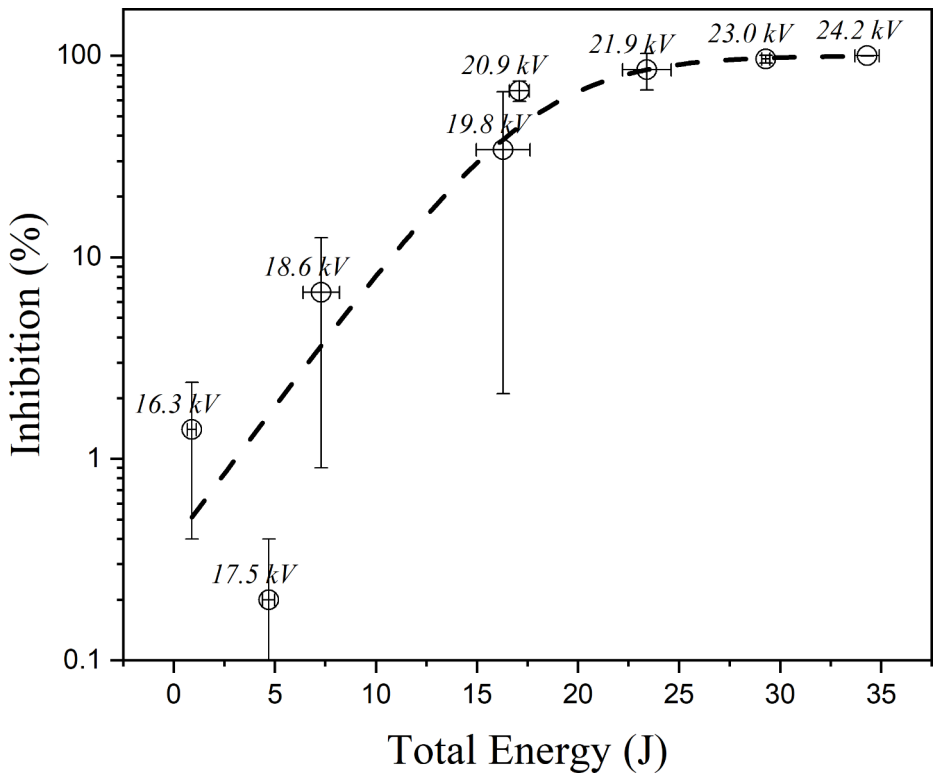| V_{pp} (kV)	E_{Burst} (mJ)	E_{Tot} (J)	Inhibition (%)	
16.3	$(6.0\pm1.50)\times10^{-2}$	0.9 ± 0.22	1.4 ± 1.0	bB
17.5	$(3.2\pm0.20)\times10^{-1}$	4.7 ± 0.30	0.2 ± 0.2	bB
18.6	$(4.8\pm0.60)\times10^{-1}$	7.3 ± 0.90	6.7 ± 5.8	bB
19.8	1.1 ± 0.09	16.3 ± 1.33	34.1 ± 32.0	aA
20.9	1.2 ± 0.03	17.1 ± 0.50	67.4 ± 7.8	aA
21.9	1.6 ± 0.08	23.4 ± 1.20	85.0 ± 12.5	aA
23.0	1.9 ± 0.02	29.3 ± 0.20	96.0 ± 4.3	aA
24.2	2.3 ± 0.04	34.3 ± 0.60	99.7 ± 3	aA

Fig. 3 Inhibition of *B. cinerea* conidial germination by a 30 s plasma treatment obtained at different ignition voltages (labels in the graph) as a function of the corresponding total plasma energy

was progressively stronger increasing the VDBD treatment time. Different responses to the treatments were recorded among the fungal species. Germination of *B. cinerea* conidia was slightly increased (1–7.2%), although with no statistical difference from the untreated control, by exposure to VDBD up to 2 s (1000 bursts) and was completely inhibited after 5 s (2500 bursts) (Fig. 4). *M. fructicola* and *F. graminearum* were slightly inhibited in conidial germination (8.1% and 6.3% respectively) after 2 s (1000 bursts) of treatment, while shorter exposure time had no effect. Although a VDBD treatment time of 5 s (2500 bursts) caused about 99% of inhibition for *M. fructicola*, 20 s (10,000 bursts) of exposure to plasma was required to obtain a complete inhibition of conidial germination for both fungi (Fig. 4). *A. alternata* was poorly affected by short time of plasma exposure showing a slight increase (1.0–2.4%) in conidial germination after 0.5 s (250 bursts) and 1 s (500 bursts), only a slight inhibition (1.0%) after 2 s (1000 bursts), while it was completely inhibited after 60 s (30,000 bursts) of treatment (Fig. 4).

    B. cinerea, and *M. fructicola*, both species belonging to the family of *Sclerotiniaceae*, showed very similar responses and were the most sensitive while *F. graminearum* and *A. alternata* were more resistant to the treatment with VDBD. No significant differences were detected at exposure time shorter than 2 s which caused very poor inhibition of fungal germination (<4%). A significant increase of the inhibitory activity (57–77%) of treatments
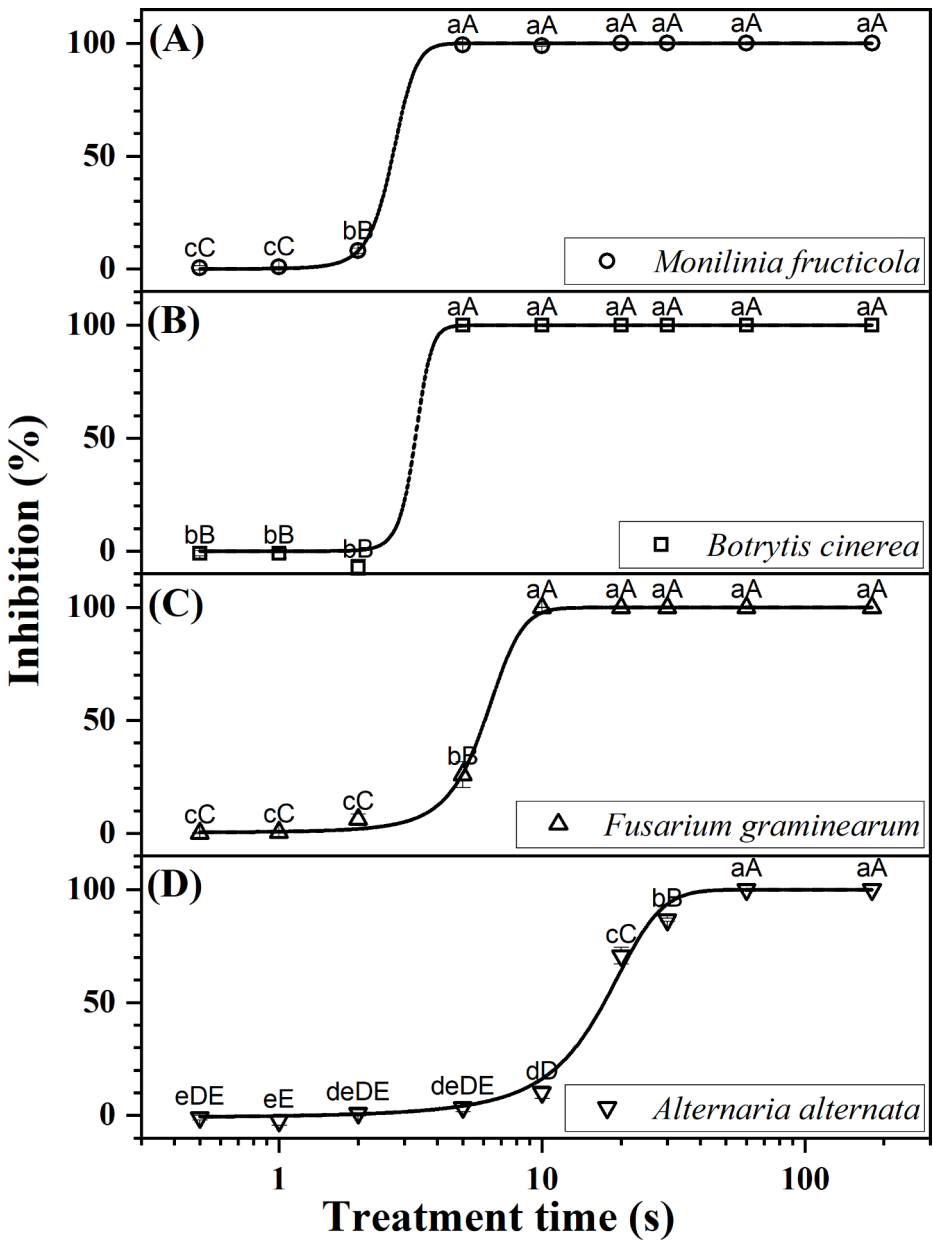
Fig. 4 Response of different fungal species to VDBD treatments in conidial germination tests. For each fungus, figures followed by a same letter are not significantly different at the probability levels $P=0.05$ (small letters) or $P=0.01$ (capital letters) according to Tukey's HSD test

was recorded at 5 and 10 s of VDBD exposure and reached complete inhibition at 60 s (Fig. 4; Table 3).

Conidial Germination Tests on Different Media

The response of *A. carbonarius* conidia to VDBD treatments was evaluated by comparing three different agarized media and different duration of plasma exposure. The statistical significance of the two principal factors and their interaction was ascertained by a two-way ANOVA analysis (Fig. 5; Table 4).

The sensitivity to VDBD treatments was significantly higher on MEA and AG compared to PDA. In detail, conidial germination was not affected up to 2 s of treatment on MEA and AG and 5 s on PDA, while it was fully inhibited after 60 s on MEA and AG and 180 s on PDA. The inhibition rate for treatment times shorter than 60 s was slightly higher for MEA compared to AG (Table 4; Fig. 5).

The analysis showed a similar behaviour of conidia that were less inhibited in their germination on the most complex medium (PDA) and at shorter treatment duration (up to 5 s), while longer treatment durations and less complex media (AG ad MEA) caused significantly higher percentages of conidial inhibition. A gradual increase in the mean inhibition rate was recorded starting from 10 s and reaching 100% at 180 s of exposure.

Cryo-SEM Imaging

Cryo-SEM high-resolution imaging showed for all the media a superficial fibrous-like microstructure composed of interconnected strands delimiting pores with a broad size distribution of up to a few micrometres (Fig. 6).

These results agree with the previous reports for similar samples [33–35]. At a coarser scale, the microstructure of the agarized media appears as a porous network made of bun-

Table 3 Two-way ANOVA test for inhibition rate (%) of conidial germination by fungal species and duration of VDBD treatment. The mean values±standard error for each level of the two factors are shown. Values followed by the same letter are not significantly different at $P=0.05$, according to Tukey's HSD

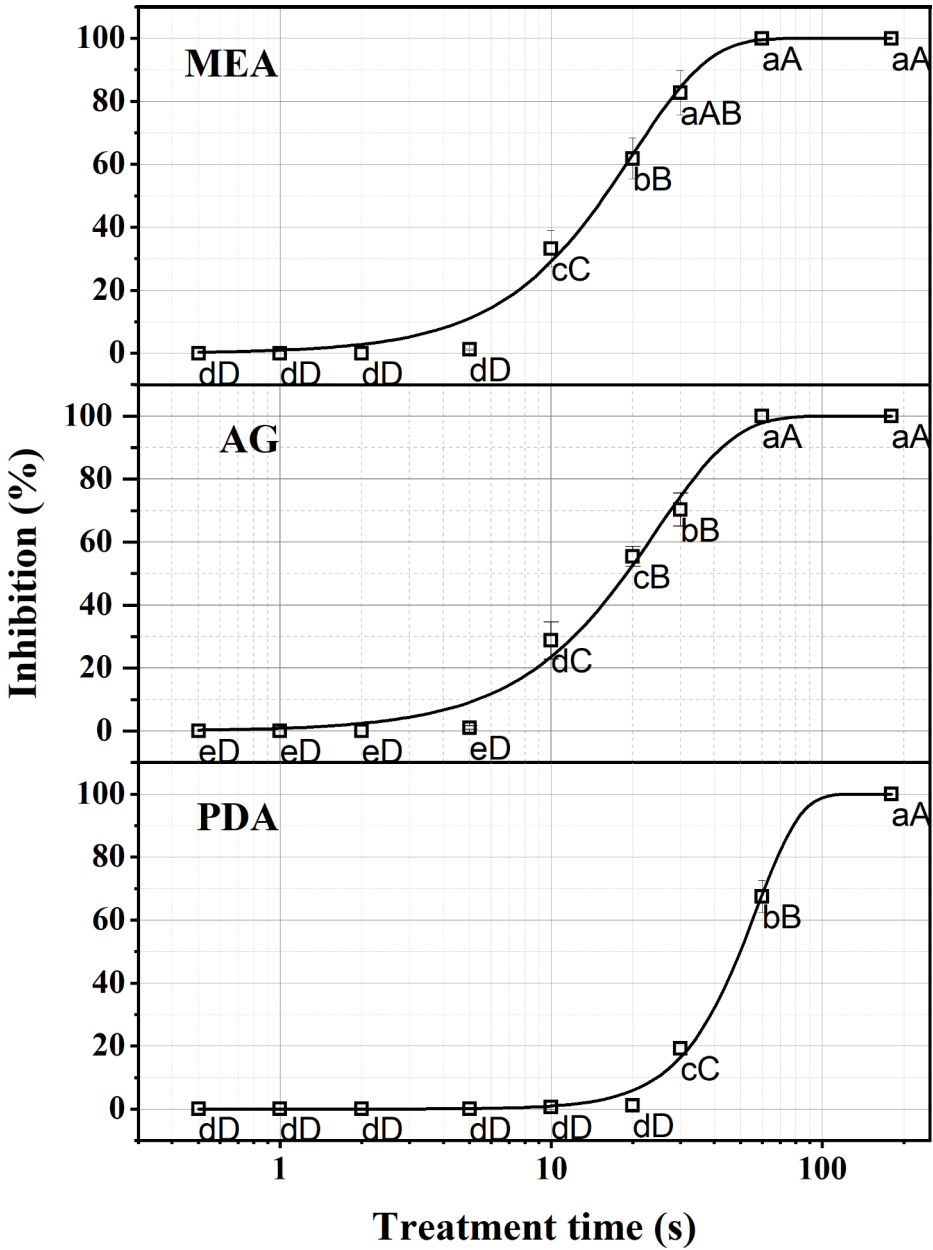| Inhibition rate (%)		
Fungal species		
A. alternata	40.9±8.6	c
F. graminearum	59.2±9.1	b
B. cinerea	65.6±9.5	a
M. fructicola	67.5±8.9	a
Exposure times (s)		
0.5	-0.3±0.4	e
1	-0.5±0.7	e
2	2.0±2.0	e
5	57.2±13.1	d
10	77.2±11.7	c
20	92.7±3.9	b
30	96.6±1.7	a
60	100.0±0.0	a
180	100.0±0.0	a

Fig. 5 Response of *A. carbonarius* to VDBD treatments in conidial germination tests

Table 4 Two-way ANOVA test for inhibition rate (%) of conidial germination by agarized media and duration of VDBD treatment. The mean values ± standard error for each level of the two factors are shown. Values followed by the same letter are not significantly different at $P = 0.05$, according to Tukey's HSD

Inhibition rate (%)		
Agarized media		
PDA	20.9 ± 6.8	b
AG	39.5 ± 7.9	a
MEA	42.0 ± 8.2	a
Exposure times (s)		
0.5	0.0 ± 0.0	f
1	0.0 ± 0.0	f
2	0.0 ± 0.0	f
5	0.7 ± 0.3	f
10	20.8 ± 5.6	e
20	39.5 ± 9.8	d
30	57.4 ± 10.0	c
60	89.2 ± 5.6	b
180	100.0 ± 0.0	a

dles of agarose helices. The presence of agaropectin in the agar starch that does not participate in the medium network, reduces the porosity making it more compact [36]. The whole polymer network was filled with free water molecules [37] and the pores of the medium microstructure showed a broad size distribution, while the mesh size varied from a few hundred nanometres to a few micrometres.

Adding non-gelling saccharides such as sucrose, glucose, and maltose, in large amounts (>5%) has been shown to impact the formation of agarose gels [38–40] and their mechanical properties [41, 42]. In our case, however, their concentration was always lower than 5%. Cryo-SEM observations of the microstructure of 2% agar media added with different non-gelling saccharides (dextrose and maltose) and potato starch are illustrated in Fig. 6. The microstructures observed become increasingly coarser as they move from MEA to AG and finally to PDA compared to those shown by WA. We believe that the increasing non-uniformity of the culture media could influence the electrical response and consequently the ignition of the plasma.

Electrical Response of Agarized Media

Due to the nature of the agarized media used in the experiments, consisting basically of a polyelectrolyte complex, the conduction is mainly via the ionic charge transport mechanisms. Therefore, the EIS technique is particularly suitable to provide insights into the elicited conducting properties [43]. The experimental results represented in terms of Nyquist Plots (NPs) are shown in Fig. 7 (full spectra) and inset herein, the latter showing the magnification of the response in the high-frequency regime.

The NPs consisted of two semicircles, the smallest, on the high-frequency side, referring to the system acting as a non-perfect capacitor, whereas the low-frequency region, refers to the electrode polarization and charge transfer current region. Both sections of the equivalent circuit can be easily simulated as the series of two parallel components made up of a constant phase element Z_{CPE} and of a resistance R. The Z_{CPE} is given by:
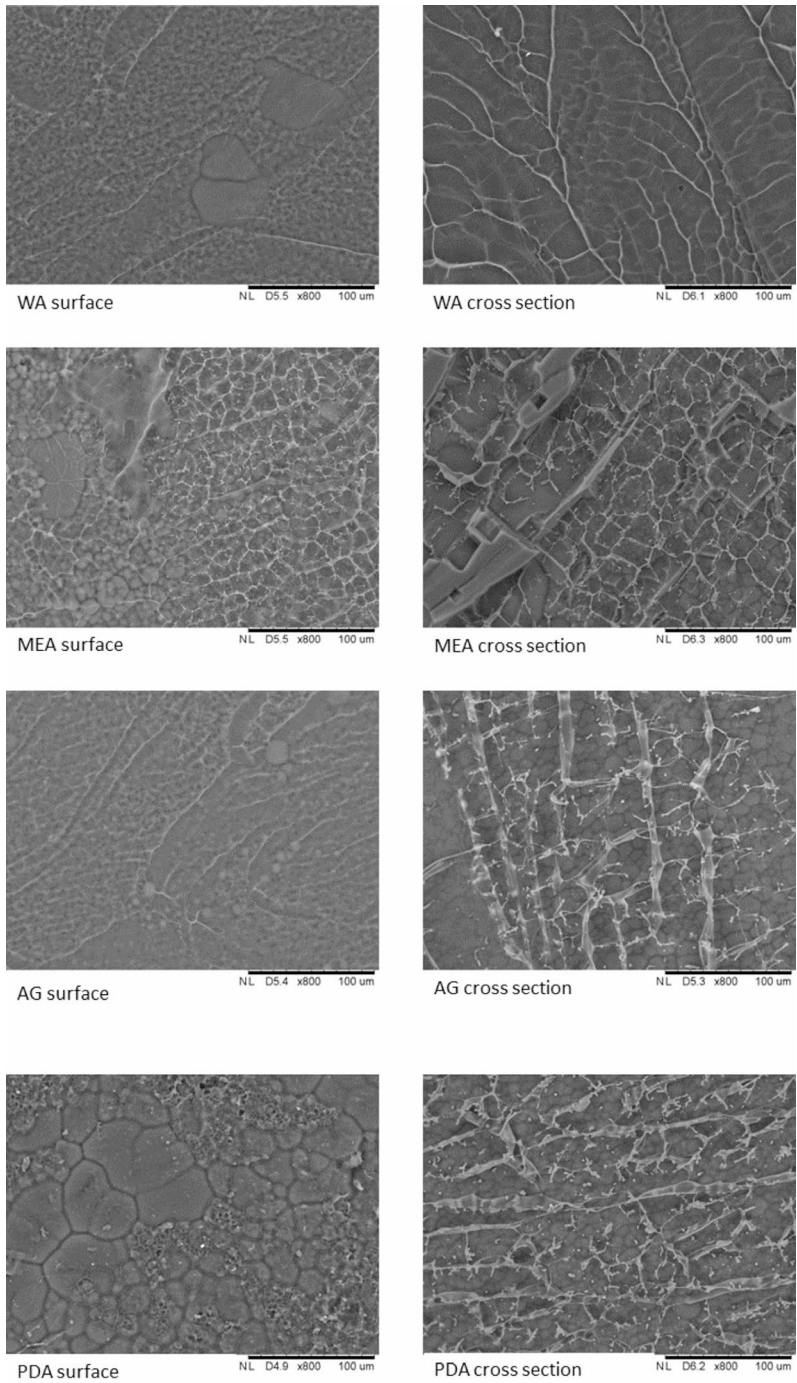
Fig. 6 Cryo-SEM images of the surface and longitudinal cross-section of different agarized media

$$Z_{CPE} = \frac{1}{Q_0 \left(j\omega\right)^n} \qquad \text{(Eq. 1)}$$

and is a phenomenological element introduced to simulate a non-perfect capacitive element [44]. The n parameter plays the main role since if it is close to zero the impedance element behaves more like a resistor, while when it is close to 1 the circuital component acts like a pure capacitor. Therefore, the n value can be a parameter giving information on the sample inhomogeneity since the closer the n values are to zero the more the items will show conductive paths where ion charges move via the ion hopping mechanism. [45]

As a first insight, in NPs representation (Fig. 7) the WA and MEA medium evidenced the highest values of the real (ReZ) and imaginary part (ImZ) of the impedance that hint at the lower ionic conductivity of these media under the AC field. These results were furthermore underlined by the values of the best-fit parameters (see Table 5) showing the highest ionic resistance, R_{ion} values of the corresponding $Z_{CPE,LF}$ term with $n=0.80-0.77$ respectively.
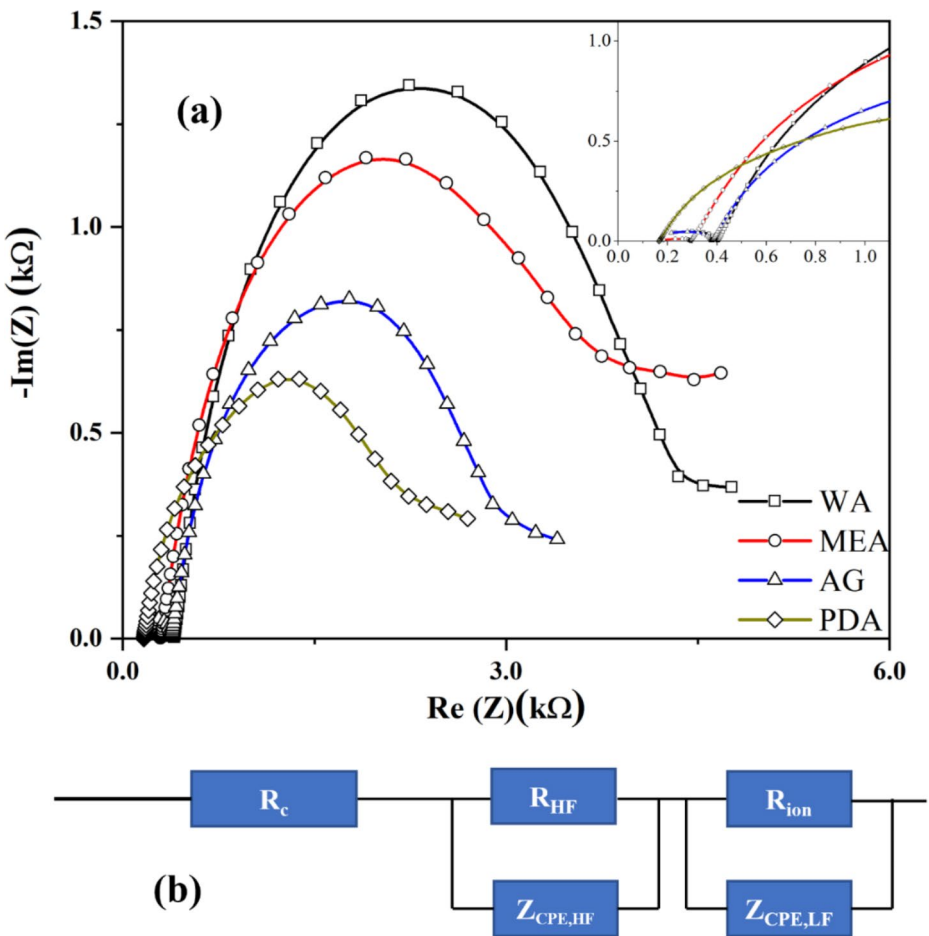
Fig. 7 (a) NPs readouts and best-fit curves for the four types of agarized media; (b) equivalent electrical circuit adopted for the best fit

Table 5 EIS Simulation parameters

Gel	$R_{ion}(\Omega)$	$Z_{CPE,LF}$	
		$Q_0\,(F^n\Omega^{(n-1)})$	n
WA	*3895*	*2.298×10^{-5}*	*0.80*
MEA	*3524*	*2.287×10^{-5}*	*0.77*
AG	*2597*	*4.218×10^{-5}*	*0.70*
PDA	*2165*	*6.759×10^{-5}*	*0.69*
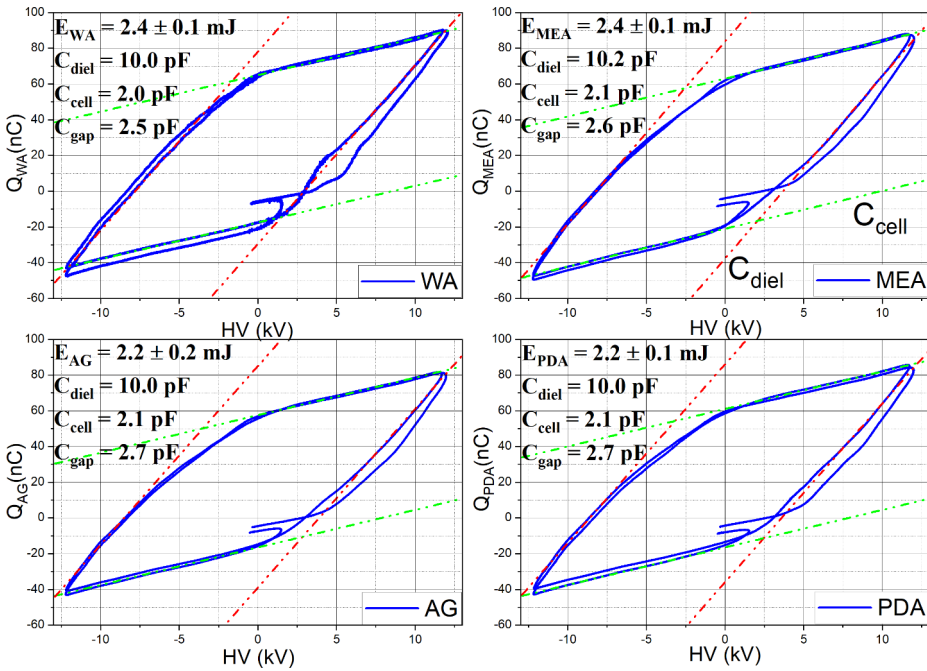
Fig. 8 Charge-Voltage Lissajous figures for the different agarized media used in this study (WA, MEA, AG and PDA). In the figures are reported the energy (E) measured for each agarized media, and the capacitance (C) of different equivalent circuit component (dielectric, cell and gap) [46]. Q-V characteristics were averaged over 100 samples, using the same applied voltage. The discharge was produced in humid air at atmospheric pressure and a fixed flow rate of 7 slm.

Interestingly, the lower resistance and n values in AG and PDA confirmed the effect of the structure inhomogeneity causing the presence of a higher density of conductive paths.

Charge Voltage Characteristics

Figure 8 shows charge-voltage (Q-V) characteristics for the discharge gap filled with disks of the different agarized media used in the present work. All the disks were 6 mm in diameter and 3 mm in height so that the DBD airgap reduces to 3 mm with a gas-treated volume of 8.5×10^{-5} cm^3 and a gas residence time in the discharge region of 12 ms, i.e. about six HV bursts.

The total energy coupled to the discharge can be evaluated by the integration of Q-V characteristics reported in Fig. 8. Slight differences were observed among the different media

used. For WA and MEA, the energy transferred per burst was around 2.4 mJ which was 10% higher than for AG and PDA media. This was evidently related to the higher charging of the surfaces exposed to plasma, and consistent with the EIS measurements observation on the culture media leading to higher discharge energy for WA and MEA and lower for AG and PDA. It is worth observing that also the shapes of the hysteresis cycles were different. In the case of WA, the Q-V diagram was close to the ideal characteristic parallelogram shape. In the other media cases, the shape was deviating from the ideal one, showing a partial almond shape. Those differences could be ascribed to the inhomogeneity and size of the porous structures observed by cryo-SEM leading to dissipative path not uniformly distributed in the bulk of the media. The increasingly complex structure of loaded agar medium, passing from MEA to AG and finally to PDA media compared with WA, translates into a gradual expansion of the plasma across the available dielectric area during the discharge phase.

From the measured energy we can estimate an energy density of 45 kJ m^{-3} for the empty case and 170 kJ m^{-3} WA/MEA and 156 kJ m^{-3} for AG/PDA. According to previously published results, we can estimate a concentration greater than 500 ppm of ozone inside the discharge region [13, 47]; however, this can be considered the maximum concentration due to the consumption of ozone precursor (oxygen atoms) and ozone itself during plasma-agar medium-water vapour interactions.

Discussions

Low-temperature plasma technology can be considered an eco-sustainable tool with several potential applications in agriculture and food production that are currently being explored. An important role of LTP application had been confirmed in the decontamination of food matrix and derivatives from major fungal pathogens responsible for postharvest decay [5, 48] and other microorganisms or their metabolites like mycotoxins [49] posing serious concern to human or animal health.

This potential for practical application of plasma technology is based on the combination of increased knowledge of mechanisms of plasma interactions with the target microorganisms and molecules, along with known risks and advances in reactor engineering and design [4]. Advantages include operation at low temperatures, short processing time, energy efficiency and high antimicrobial efficacy with minimal impact on product quality and the environment [4].

The exact mechanisms of antimicrobial activity of plasma treatment remain unclear [50–52]; however, it is hypothesized that it mainly acts directly on the pathogen itself. The impact of plasma on microbes, in general, includes cell damage such as alteration of the permeability of cell membrane, subsequent leakage of cellular components, critical damage to intracellular organelles or proteins, and disruption of DNA, possibly by UV radiation generated during recombination of plasma reactive species.

The efficacy against microorganisms is however dependent on the target species. In a previous study, we evaluated the in vitro direct inhibitory effect of non-contact Surface Dielectric Barrier Discharge on conidial germination of different fungal species [5]. Due to the intrinsic non-contact nature of the applied plasma, we could assume that antimicrobial activity can be attributed mainly to RONS and UV light emission. This translates into processes involving reactions between cell envelopes and chemical species resulting in the

cell wall and membrane damage inducing cell apoptosis. Another point was related to the evident correlation between efficacy and the cellular structure of fungal species, requiring treatment time to be increased from simple unicellular structure to multicellular and/or melanized spores.

In this work, we evaluated the effectiveness of the inhibitory effect of VDBD treatments to further investigate different responses of five selected fungal species. Compared to SDBD used in our previous study [5], the plasma can enable different mechanisms for decontamination. In fact, the samples in a VDBD are permeated by the plasma and exposed directly to the full emission spectra of an air discharge which include UV/VIS/NIR radiations. Moreover, the direct impact of locally produced ions and electrons, radical and atomic species, such as atomic oxygen, is more efficient than the SDBD case [5]. Several factors were explored to evaluate their influence on the inhibitory effect. Discharge characteristics (i.e., such as energy, treatment time, plasma emission) and target characteristics (i.e., the microorganisms and the substrates) were studied during the experiments. Emission spectroscopy from neutral molecular nitrogen and its positive ion revealed the presence of a strong electric field applied to the samples especially when the discharge polarity makes the agarized media the temporary anode. From spectroscopic observation of the SPS(0,0) band of molecular nitrogen, a possible thermal effect on the surface cannot be excluded even though, due to the filamentary character of the discharge, this should be a local effect confined to the impact region of the filament. This fast gas heating is taking place on a time scale of hundreds of nanoseconds and the sample are exposed to fast heat shocks. Nevertheless, we must point out that on average the gas temperature is close to room temperature in the after-burst, also because of the short residence time of the air carrier gas in the discharge region. In fact, at the beginning of each new burst, the gas temperature is close to room one. Consequently, temperature should not be the main physical agent responsible for decontamination as evidenced by SPS(0.0) band emission. The visual observation of samples after treatment does support this conclusion being the shape and the surface of the samples well preserved. Moreover, since no melting of the agarized media sample was observed, we can infer that the heat transfer was fast and not sufficient to cause state transition.

In vitro, the efficacy of VDBD treatments was determined in conidial germination tests with five different fungi using different exposure times and agarized media. A standard method commonly applied to evaluate the responses of fungi to treatments was used (e.g., [5, 53]). The use of defined agarized media with known and uniform composition reduces variability in growing conditions among samples that is difficult to control using other more natural substrates like plant materials. In these controlled conditions, we were able to explore key parameters that may influence the inhibitory effect of VDBD on the tested fungi and compare them for their responses to the treatments.

We showed that the electrical response of the discharge apparatus in the presence of different agarized media used for conidial germination tests does not change significantly in terms of plasma energy, but we could observe differences in the shape of the Lissajous figures. The WA and MEA media showed an almost ideal shape suggesting that the plasma ignition across the gap is uniform with the selected applied voltage. The other more complex agarized media (AG, and PDA), instead, showed an almond shape that can be explained with a non-uniform medium morphology due to their intrinsic composition. This hypothesis is supported by the cryo-SEM observation of medium surfaces and cross-sections, showing different porosity and pore size. Furthermore, the electrical behaviour of the media mea-

sured by EIS spectroscopy evidenced a more capacitive behaviour of WA and MEA with respect to AG and PDA, thus leading to higher charge accumulation on the treated surface samples and consequently more energy available for the discharge channel. Moreover, EIS measurements suggest the presence of dissipative path in the bulk of the more complex media. The plasma will then ignite at different times and in different positions on the surface since the breakdown criteria are not the same everywhere. This could be a possible explanation of differences observed in the time required for reaching a complete inhibition of conidial germination on media different from WA and the observed non-uniform inactivation in short-time treatments.

Comparison of treatments performed on different fungal species with the same agarized media and same plasma treatment conditions can evidence the effect of different morphological features (e.g., number of cells per spore, irregular spore surface), cell structures (i.e., thickness and composition of the cell wall), and metabolic pathways (pigment biosynthesis, antioxidant and detoxification systems) of fungi. Melanized fungi are more resistant than those non-melanized to UV light-induced and oxidant-mediated damages, extremes temperature, hydrolytic enzymes, heavy metal toxicity, and antimicrobial drugs [5, 54]. *B. cinerea* and *M. fructicola*, belonging to the same taxonomic family (*Sclerotiniaceae*), with unicellular conidia and similar melanin profiles, showed similar responses to plasma treatments, being completely inhibited after 5 and 20 s of plasma exposure, respectively. In the case of *B. cinerea* a slight increase of conidial germination (up to 7.2%) was recorded following brief treatments (up to 2s) that was likely due to initial plasma-induced cell-wall loosening. For more prolonged treatment cell damages became irreversible and caused death. *F. graminearum* and *A. alternata* with multicellular conidia were more resistant to the plasma treatment, also in relation to their melanization, and germination was completely inhibited by 20 and 60 s exposure time, respectively. *A. carbonarius* conidia, unicellular and more melanized than those of the other fungi, were fully inhibited by 60 s of plasma exposure. The rate of inhibition of *A. carbonarius* was depending on the type of agarized medium used. The nutrient richness of the medium influenced the inhibitory effect of the treatment, and this may be attributed to the inhomogeneity of the rich media influencing the plasma ignition on the sample surface. PDA, the most complex medium among those tested, hindered more than others the efficacy of plasma treatment against *A. carbonarius* and conidial germination was completely inhibited only after 180 s of plasma exposure.

Conclusions

In summary, the utilization of low-temperature plasma holds promise in the management of fungal species, including causal agents of postharvest diseases and mycotoxigenic fungi [5]. The findings presented in this study were focused on the effects of various factors on the antimicrobial effectiveness of VDBD on five phytopathogenic and mycotoxigenic fungi. To achieve this, a range of diagnostic techniques was employed to characterize both the plasma phase and its interaction with agarized media.

Under consistent plasma experimental conditions, i.e. reactor geometry and substrate materials, the initial step was to define plasma parameters, primarily the input energy. In our experiment, this was crucial to ensure comprehensive coverage of the targeted region by the plasma. The inclusion of agarized media on the grounded electrode introduced an asym-

metrical aspect to the plasma behaviour. This was particularly evident from emission spectroscopy during the negative polarity half cycle, indicating elevated emission and higher E/N values.

Ultimately, the success of the treatment was closely dependent on the biological traits, such as the complexity of fungal spores, in terms of cell numbers and melanization, which yield distinct responses to plasma exposure. In this context, the primary experimental parameter was the duration of exposure to plasma, i.e., the total applied energy. Furthermore, the electrical characteristics of media with varying compositions, as revealed through EIS spectroscopy, also influenced treatment efficacy, likely due to shifts in plasma behavior, as illustrated by charge-voltage Lissajous figures.

Our findings strongly suggest that the treatment intensity must be selected accordingly to the particular matrix to be treated, indicating that decontamination protocols must be defined prior to any actual application on food matrices.

Data Availability All data generated or analysed during this study are included in this published article.

Declarations

Competing Interests The authors declare no competing interests.

Ethical Approval Not applicable.

References

1. Turner M (2016) Physics of Cold plasma. Cold plasma in Food and Agriculture. Elsevier, pp 17–51

2. Pankaj SK, Bueno-Ferrer C, Misra NN et al (2014) Applications of cold plasma technology in food packaging. Trends Food Sci Technol 35:5–17. https://doi.org/10.1016/j.tifs.2013.10.009
3. Ambrico PF, Šimek M, Morano M et al (2017) Reduction of microbial contamination and improvement of germination of sweet basil (Ocimum basilicum L.) seeds via surface dielectric barrier discharge. J Phys D Appl Phys 50:305401. https://doi.org/10.1088/1361-6463/aa77c8
4. Bourke P, Ziuzina D, Boehm D et al (2018) The potential of Cold plasma for safe and sustainable Food production. Trends Biotechnol 36:615–626. https://doi.org/10.1016/j.tibtech.2017.11.001
5. Ambrico PF, Šimek M, Rotolo C et al (2020) Surface Dielectric Barrier Discharge plasma: a suitable measure against fungal plant pathogens. Sci Rep 10:1–17. https://doi.org/10.1038/s41598-020-60461-0
6. Misra NN, Keener KM, Bourke P et al (2014) In-package atmospheric pressure cold plasma treatment of cherry tomatoes. J Biosci Bioeng 118:177–182. https://doi.org/10.1016/j.jbiosc.2014.02.005
7. Dasan BG, Boyaci IH, Mutlu M (2016) Inactivation of aflatoxigenic fungi (aspergillus spp.) on granular food model, maize, in an atmospheric pressure fluidized bed plasma system. Food Control 70:1–8. https://doi.org/10.1016/j.foodcont.2016.05.015
8. Keener KMM, Misra NNN (2016) Future of Cold plasma in Food Processing. Elsevier Inc
9. Devi Y, Thirumdas R, Sarangapani C et al (2017) Influence of cold plasma on fungal growth and aflatoxins production on groundnuts. Food Control 77:187–191. https://doi.org/10.1016/j.foodcont.2017.02.019
10. Henson JM, Butler MJ, Day AW (1999) The Dark side of the Mycelium: Melanins of Phytopathogenic Fungi. Annu Rev Phytopathol 37:447–471. https://doi.org/10.1146/annurev.phyto.37.1.447
11. Yu J-H, Keller N (2005) Regulation of secondary metabolism in Filamentous Fungi. Annu Rev Phytopathol 43:437–458. https://doi.org/10.1146/annurev.phyto.43.040204.140214
12. Gao Q, Garcia-Pichel F (2011) Microbial ultraviolet sunscreens. Nat Rev Microbiol 9:791–802. https://doi.org/10.1038/nrmicro2649
13. Ambrico PF, Šimek M, Ambrico M et al (2020) On the air atmospheric pressure plasma treatment effect on the physiology, germination and seedlings of basil seeds. J Phys D Appl Phys 53:104001. https://doi.org/10.1088/1361-6463/ab5b1b
14. Barsoukov E, Macdonald JR (2005) Impedance Spectroscopy: Theory, Experiment, and Applications, 2nd Edition. In: Impedance Spectroscopy: Theory, Experiment, and Applications, 2nd Ed. J. Wiley & Sons, Inc., Hoboken, New Jersey
15. Ragoisha GA, Bondarenko AS (2003) Potentiodynamic electrochemical impedance spectroscopy for solid state chemistry. 91
16. Bondarenko AS, Ragoisha GA Eis Spectrum Analyser. In: http://www.abc.chemistry.bsu.by/vi/analyser/. http://www.abc.chemistry.bsu.by/vi/analyser/
17. Voráč J, Synek P, Procházka V, Hoder T (2017) State-by-state emission spectra fitting for non-equilibrium plasmas: OH spectra of surface barrier discharge at argon/water interface. J Phys D Appl Phys 50:294002. https://doi.org/10.1088/1361-6463/aa7570
18. Voráč J, Synek P, Potočňáková L et al (2017) Batch processing of overlapping molecular spectra as a tool for spatio-temporal diagnostics of power modulated microwave plasma jet. Plasma Sources Sci Technol 26:025010. https://doi.org/10.1088/1361-6595/aa51f0
19. Voráč J, Kusýn L, Synek P (2019) Deducing rotational quantum-state distributions from overlapping molecular spectra. Rev Sci Instrum 90:123102. https://doi.org/10.1063/1.5128455
20. Dilecce G (2014) Optical spectroscopy diagnostics of discharges at atmospheric pressure. Plasma Sources Sci Technol 23:015011. https://doi.org/10.1088/0963-0252/23/1/015011
21. Dilecce G, Ambrico PF, Benedictis S, De (2007) New N_2 ($C^3\Pi_u$, v) collision quenching and vibrational relaxation rate constants: 2. PG emission diagnostics of high-pressure discharges. Plasma Sources Sci Technol 16:S45–S51. https://doi.org/10.1088/0963-0252/16/1/S04
22. Dilecce G, Ambrico PF, Martini LM, Tosi P (2022) On the determination of the vibrational temperature by optical emission spectroscopy. Plasma Sources Sci Technol 31:077001. https://doi.org/10.1088/1361-6595/ac7f54
23. Dilecce G, Ambrico PF, De Benedictis S (2010) On the collision quenching of $N_2^+(B,^2S_u^+$, $v = 0)$ by N_2 and O_2 and its influence on the measurement of E / N by intensity ratio of nitrogen spectral bands. J Phys D Appl Phys 43:195201. https://doi.org/10.1088/0022-3727/43/19/195201
24. Pancheshnyi SV, Starikovskaia SM, Starikovskii AY (1998) Measurements of rate constants of the $N_2(C^3\Pi_u,v'=0)$ and $N_2^+(B^2\Sigma_u^+,v'=0)$ deactivation by N_2, O_2, H_2, CO and H_2O molecules in afterglow of the nanosecond discharge. Chem Phys Lett 294:523–527. https://doi.org/10.1016/S0009-2614(98)00879-3
25. Hagelaar GJM, Pitchford LC (2005) Solving the Boltzmann equation to obtain electron transport coefficients and rate coefficients for fluid models. Plasma Sources Sci Technol 14:722–733. https://doi.org/10.1088/0963-0252/14/4/011
26. Dijcks S, Kusýn L, Janssen J et al (2023) High-resolution electric field and temperature distributions in positive streamers. Front Phys 11. https://doi.org/10.3389/fphy.2023.1120284

27. Kozlov KV, Wagner H, Brandenburg R, Michel P (2001) Spatio-temporally resolved spectroscopic diagnostics of the barrier discharge in air at atmospheric pressure. J Phys D Appl Phys 34:3164–3176. https://doi.org/10.1088/0022-3727/34/21/309

28. Paris P, Aints M, Valk F et al (2005) Intensity ratio of spectral bands of nitrogen as a measure of electric field strength in plasmas. J Phys D Appl Phys 38:3894–3899. https://doi.org/10.1088/0022-3727/38/21/010

29. Pancheshnyi SV, Starikovskaia SM, Starikovskii AY (1998) Measurements of rate constants of the N2(C$^3\Pi_u$, $v' = 0$) and N$_2^+$(B$^2\Sigma_u^+$, $v' = 0$) deactivation by N$_2$, O$_2$, H$_2$, CO and H$_2$O molecules in afterglow of the nanosecond discharge. Chem Phys Lett 294. https://doi.org/10.1016/S0009-2614(98)00879-3

30. Dilecce G, Ambrico PF, De Benedictis S (2010) On the collision quenching of N$_2^+$(B$^2\sum_u^+$, $v = 0$) by N$_2$ and O$_2$ and its influence on the measurement of E/N by intensity ratio of nitrogen spectral bands. J Phys D Appl Phys 43. https://doi.org/10.1088/0022-3727/43/19/195201

31. Kozlov KV, Wagner H-E (2007) Progress in Spectroscopic Diagnostics of Barrier Discharges. Contrib Plasma Phys 47:26–33. https://doi.org/10.1002/ctpp.200710005

32. Bilek P, Obrusnik A, Hoder T et al (2018) Electric field determination in air plasmas from intensity ratio of nitrogen spectral bands: II. Reduction of the uncertainty and state-of-the-art model. Plasma Sources Sci Technol 27

33. Charlionet R, Levasseur L, Malandain J-J (1996) Eliciting macroporosity in polyacrylamide and agarose gels with polyethylene glycol. Electrophoresis 17:58–66. https://doi.org/10.1002/elps.1150170111

34. Brigham JE, Gidley MJ, Hoffmann RA, Smith CG (1994) Microscopic imaging of network strands in agar, carrageenan, locust bean gum and kappa carrageenan/locust bean gum gels. Food Hydrocoll 8:331–344. https://doi.org/10.1016/S0268-005X(09)80345-7

35. Nishinari K, Fang Y (2017) Relation between structure and rheological/thermal properties of agar. A mini-review on the effect of alkali treatment and the role of agaropectin. Food Struct 13:24–34. https://doi.org/10.1016/j.foostr.2016.10.003

36. Medin AS (1995) Studies on Structure and Properties of Agarose (Comprehensive Summaries of Uppsala Dissertations from the Faculty of Science & Technology)

37. Woessner DE, Snowden BS, Chiu Y-C (1970) Pulsed nmr study of the temperature hysteresis in the agar-water system. J Colloid Interface Sci 34:283–289. https://doi.org/10.1016/0021-9797(70)90180-3

38. Nishinari K, Watase M, Kohyama K et al (1992) The effect of sucrose on the Thermo-Reversible Gel-Sol transition in agarose and gelatin. Polym J 24:871–877. https://doi.org/10.1295/polymj.24.871

39. Russ N, Zielbauer BI, Koynov K, Vilgis TA (2013) Influence of Nongelling Hydrocolloids on the Gelation of Agarose. Biomacromolecules 14:4116–4124. https://doi.org/10.1021/bm4012776

40. Watase M, Kohyama K, Nishinari K (1992) Effects of sugars and polyols on the gel-sol transition of agarose by differential scanning calorimetry. Thermochim Acta 206:163–173. https://doi.org/10.1016/0040-6031(92)85294-6

41. Watase M, Nishinari K, Williams PA, Phillips GO (1990) Agarose gels: effect of sucrose, glucose, urea, and guanidine hydrochloride on the rheological and thermal properties. J Agric Food Chem 38:1181–1187. https://doi.org/10.1021/jf00095a005

42. Normand V (2003) Effect of sucrose on agarose gels mechanical behaviour. Carbohydr Polym 54:83–95. https://doi.org/10.1016/S0144-8617(03)00153-X

43. Nwanya AC, Amaechi CI, Udounwa AE et al (2015) Complex impedance and conductivity of agar-based ion-conducting polymer electrolytes. Appl Phys a Mater Sci Process 119. https://doi.org/10.1007/s00339-014-8979-x

44. Gorrec B, Le, Montella C (2010) Handbook of Electrochemical Impedance Spectroscopy. Electrical Circuit containing CPEs. Transformation 1–30. https://doi.org/10.13140/RG.2.2.11979.62245

45. Lee CJ, Wu H, Hu Y et al (2018) Ionic conductivity of polyelectrolyte hydrogels. ACS Appl Mater Interfaces 10. https://doi.org/10.1021/acsami.7b15934

46. Kogelschatz U (2003) Dielectric-barrier discharges: their history, Discharge Physics, and Industrial Applications. Plasma Chem Plasma Process 23:1–46. https://doi.org/10.1023/A:1022470901385

47. Zhang Y, Wei L, Liang X, Šimek M (2019) Ozone production in Coaxial DBD using an amplitude-modulated AC Power Supply in Air. Ozone Sci Eng 00:1–11. https://doi.org/10.1080/01919512.2019.1565986

48. Rana S, Mehta D, Bansal V et al (2020) Atmospheric cold plasma (ACP) treatment improved in-package shelf-life of strawberry fruit. J Food Sci Technol 57:102–112. https://doi.org/10.1007/s13197-019-04035-7

49. Hojnik N, Cvelbar U, Tavčar-Kalcher G et al (2017) Mycotoxin Decontamination of Food: Cold Atmospheric pressure plasma versus classic decontamination. Toxins (Basel) 9:151. https://doi.org/10.3390/toxins9050151

50. Yu H, Perni S, Shi JJ et al (2006) Effects of cell surface loading and phase of growth in cold atmospheric gas plasma inactivation of Escherichia coli K12. J Appl Microbiol 101:1323–1330. https://doi.org/10.1111/j.1365-2672.2006.03033.x

51. Mai-Prochnow A, Murphy AB, McLean KM et al (2014) Atmospheric pressure plasmas: infection control and bacterial responses. Int J Antimicrob Agents 43:508–517. https://doi.org/10.1016/j.ijantimicag.2014.01.025
52. Guo J, Huang K, Wang J (2015) Bactericidal effect of various non-thermal plasma agents and the influence of experimental conditions in microbial inactivation: a review. Food Control 50:482–490. https://doi.org/10.1016/j.foodcont.2014.09.037
53. De Miccolis Angelini RM, Masiello M, Rotolo C et al (2014) Molecular characterisation and detection of resistance to succinate dehydrogenase inhibitor fungicides in Botryotinia fuckeliana (Botrytis cinerea). Pest Manag Sci 70. https://doi.org/10.1002/ps.3748
54. Butler MJ, Day AW (1998) Fungal melanins: a review. Can J Microbiol 44:1115–1136. https://doi.org/10.1139/w98-119

Publisher's Note Springer Nature remains neutral with regard to jurisdictional claims in published maps and institutional affiliations.

Authors and Affiliations

Palma Rosa Rotondo[1] · Domenico Aceto[2] · Caterina Rotolo[1] · Marianna Ambrico[2] · Giorgio Dilecce[2] · Francesco Faretra[1] · Rita Milvia De Miccolis Angelini[1] · Paolo Francesco Ambrico[2]

✉ Rita Milvia De Miccolis Angelini
  ritamilvia.demiccolisangelini@uniba.it

✉ Paolo Francesco Ambrico
  paolofrancesco.ambrico@cnr.it

1 Department of Soil, Plant and Food Sciences, University of Bari ALDO MORO, Bari, Italy

2 National Research Council of Italy, Institute for Plasma Science and Technology (CNR-ISTP), Bari, Italy